

Formation of Micronuclei Responsible for Decompression Sickness

VINCENT STUART JAMES CRAIG

Department of Chemistry, The Faculties, and Department of Applied Mathematics, Research School of Physical Sciences and Engineering, The Australian National University, Canberra, ACT 0200, Australia

Received February 27, 1996; accepted May 15, 1996

In this report, the origin of micronuclei responsible for the onset of decompression sickness is investigated. The formation of cavities by tribonucleation between hydrophobic and hydrophilic surfaces has been studied using a new force measuring device, LLIFE (Light Lever Instrument for Force Evaluation). Using this instrument, the interaction force between silica surfaces in equilibrium with the cationic surfactant cetylpyridinium chloride has been measured above and below the critical micelle concentration. A long range hydrophobic attraction is evident between adsorbed monolayers and a DLVO repulsion is apparent between adsorbed bilayers. It is shown that the formation of cavities on separation occurs not only between hydrophobic monolayers but between hydrophilic bilayers, should the bilayers be squeezed sufficiently to cause rupture. The demonstration that cavities may arise upon separation between bilayers is new and leads to the postulate that cavities are formed *in vivo* by the rupture of cell membrane bilayers, thereby providing the nucleation sites for bubble formation should sufficient gas supersaturation occur. © 1996 Academic Press, Inc.

Key Words: cetylpyridinium chloride; decompression sickness; 1-hexadecyl-pyridinium chloride; hydrophobic interaction; micronuclei; tribonucleation.

INTRODUCTION

Decompression sickness or the bends has long been attributed to the formation *in vivo* of damaging gas bubbles. These bubbles are formed when tissue is supersaturated with dissolved gas to the extent where bubbles are formed as a path to equilibrium. Despite the growth of diving as a recreational activity the current best practice diving tables still have no sound theoretical basis. Adverse long-term health effects may be suffered even in the absence of any short term decompression sickness. It has been suggested that bubbles form and circulate in the body before any symptoms appear (1).

The problem lies in the fact that the bubbles causing decompression sickness are formed well below the theoretical supersaturation limits for both homogeneous (320 atm) and heterogeneous (120–180 atm) nucleation (2). While the experimental supersaturations required to produce nucleation in water at 100 to 300 atm are less than those predicted

theoretically, they are nearly two orders of magnitude higher than the degree of supersaturation that results in decompression sickness, which is less than 3 atmospheres (3–5). It is known that the nucleation of bubbles at a hydrophobic surface is more favorable, but this alone cannot account for the difference.

The difference is explained by the existence of preformed micronuclei in solution (6–8). It seems clear that if these nuclei are removed, by application of extremely high pressure or by continued boiling or evacuation, nucleation is avoided (9). However, the origin of these micronuclei is yet to be adequately explained. Several suggestions exist in the literature (10–12).

Evans and Walder (6) have demonstrated that shrimp which have been treated to remove micronuclei are more prone to bubble formation upon decompression if rapid muscular contractions have taken place. This suggests that muscular contractions of the shrimps produce micronuclei, which then lead to bubble formation. Also, micronuclei may be formed when physical damage to tissue occurs. Harvey *et al.* (8) describe a procedure which eliminates micronuclei from excised tissue, but upon physical damage to the tissue, bubbles are formed. Ikels (11), using supersaturated olive oil and glycerol/water systems, has shown that bubbles can be nucleated mechanically by tribonucleation, the process where solid bodies immersed in a liquid make and break contact, leading to the formation of nuclei. However, the wetting behavior of the surfaces used was not determined. Force measurements between hydrophobic surfaces reveal a long-range attraction, the mechanism of which is still unknown (13, 14). Upon separation of the hydrophobic surfaces a bridging vapor cavity has been observed for highly hydrophobic surfaces (15–17). These results suggest that tribonucleation is involved in the mechanism that produces micronuclei. Exercise induces mechanical stress in body tissues, causing hydrophobic surfaces to be brought together and separated on a submicroscopic scale. This process could then form cavities which would be able to nucleate bubble growth, should the solution be or become supersaturated with dissolved gases. That bends symptoms are prevalent in the limbs (6), where most mechanical stress is produced

during exercise, offers some support for such a mechanism. However, extracellular hydrophobic surfaces within the body are unlikely to be common; cell membranes consist largely of negatively charged lipids aggregated into bilayers and coated in a glycocalyx and as such are hydrophilic. Tribonucleation is unlikely to occur between bilayers due to their hydrophilic nature, but rupture of the bilayers under mechanical stress may expose hydrophobic regions which are more favorable to cavity formation.

A force measuring device has been used to investigate the processes that occur as two like surfaces are brought into contact and subsequently separated. The surfaces have been modified by the adsorption of the cationic surfactant cetylpyridinium chloride (CPCI). At low surfactant concentration a monolayer of adsorbed surfactant is formed at each surface, which renders the silica surfaces hydrophobic. At higher surfactant concentration a simple model of a cell membrane can be simulated with the completion of a fully packed bilayer on each surface, in which case the surfaces are hydrophilic.

CPCI is a biologically active molecule that is bactericidal (18–20), haemolytic (21), immunosuppressive, and toxic. This behavior is a direct consequence of its amphiphilic nature and positively charged head group. In addition to its medicinal importance, CPCI is industrially important for its detergent action. It is used in flotation (22, 23) and a wide variety of other processes where a positively charged surfactant is advantageous.

MATERIALS AND METHODS

An instrument we have recently developed (LLIFE) has been used to investigate the interaction between surfactant coated silica surfaces. The instrument, represented in Fig. 1, employs the light-lever technique employed by the atomic force microscope (AFM) (24, 25) and is described briefly below and more fully elsewhere (Craig *et al.*, submitted for publication).

The deflection of a cantilever spring is monitored as a function of separation between a silica sphere and a flat. The sphere is glued to the tip of the spring which is mounted in a fluid cell above the flat sample surface. The flat is mounted on a piezoelectric crystal, enabling separation of the surfaces to be controlled to <1 nm by application of a voltage to expand and contract the piezo tube. Spring deflection is monitored by the movement of a laser spot, reflected from the back of the spring, across a split diode. The raw data consist of (i) a dimensionless value, related to the spring deflection, derived from the diode, $(A - B)/(A + B)$ (where A and B are the voltages generated at each half of the diode), and (ii) the voltage applied to the piezo tube used to displace the flat substrate. These data are scaled in the usual manner (26). The compliance region where the tip of the spring and the flat are moving in unison is used to calibrate the diode

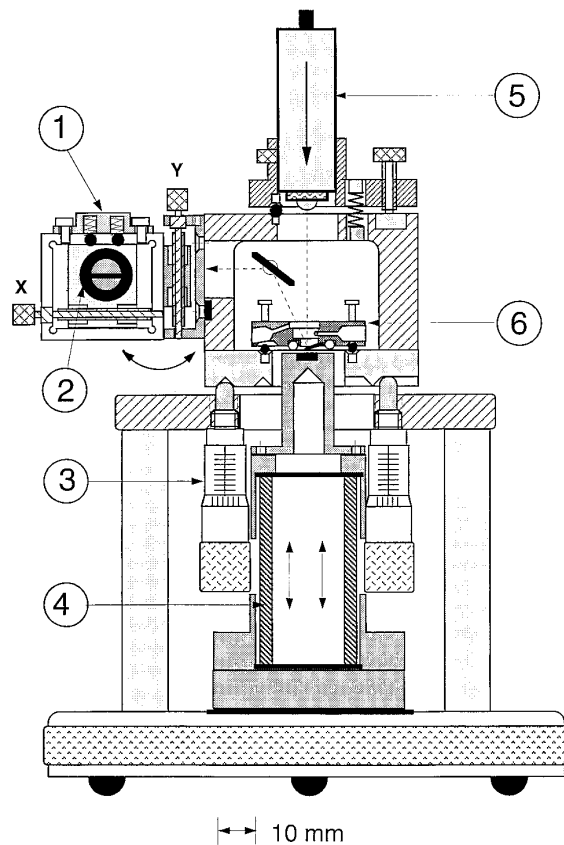


FIG. 1. Light lever instrument for force evaluation (LLIFE): (1) miniature X, Y translation stage, (2) split photodiode, (3) micrometer, (4) piezoelectric tube, (5) laser, and (6) cantilever spring mounted in fluid cell.

response and the raw separation data are adjusted to correct for deflection of the spring. The spring deflection is multiplied by the spring constant and divided by the probe radius to yield the force normalized by the radius (F/R). Solutions in equilibrium with atmospheric pressure were used. Air bubbles were removed from the syringe prior to slow injection of the solution, to reduce the possibility of gas supersaturation. Interaction forces were measured at $22^\circ\text{C} \pm 2^\circ\text{C}$, above the measured Krafft temperature for CPCI of $6^\circ \pm 1^\circ\text{C}$, suggesting that the hydrocarbon tails remain fluid under the experimental conditions.

Interaction forces between a silica flat and a silica sphere (Polysciences, ~ 20 μm diameter) were measured in aqueous solutions containing the cationic surfactant cetylpyridinium chloride (CPCI) [1-hexadecyl-pyridinium chloride [123-03-5]], supplied by Sigma, 98% pure. The flat and sphere were plasma treated (0.65 Torr H_2O , 0.10 Torr Ar, 10 W, 45 s) to ensure cleanness and complete hydroxylation of the silica surfaces. All water used in these experiments was passed through a coarse lamb's wool filter, a reverse osmosis membrane, and an activated charcoal column before single distillation and storage in a laminar flow cabinet. Force measurements were conducted using silica surfaces

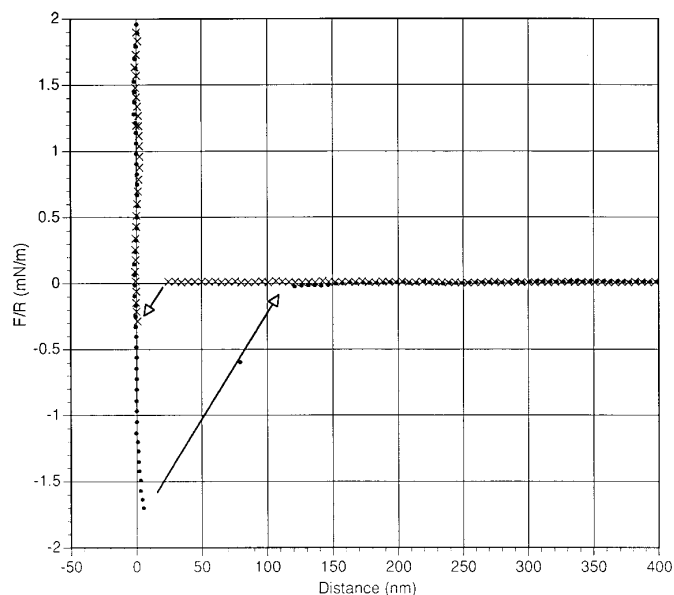


FIG. 2. An interaction curve measured on approach (crosses) and separation (dots) between silica surfaces immersed in a solution of 5.0×10^{-6} M CPCI and 0.1 M NaCl. A monolayer of surfactant coats each silica surface, rendering it hydrophobic. The type of interaction varies and may be divided into two categories. The interaction shown is representative of the first category, where small jumps and simple adhesion profiles occur. On approach no interaction is seen until a sudden jump into contact occurs from approximately 23 nm (see arrow). On separation an adhesion is seen prior to sudden separation of the surfaces and a return to zero force. Figure 3 depicts the other category of interaction seen. The cantilever spring used had a spring constant of 0.18 N/m and the radius of the probe was 11.3 μm .

that were allowed to equilibrate with the solution for 12 h for solutions of 5.0×10^{-6} M CPCI in 0.1 M NaCl and for 2.5 h for solutions of 0.001 M CPCI.

The silica sphere was fixed to a Nanoscope Si_3N_4 cantilever of spring constant 0.18 N/m, using epikote resin following the method developed by Ducker *et al.* (27). Spring constants of a number of cantilevers from each wafer were determined using the method of Cleveland *et al.* (28) and the average spring constant was used to scale the forces. The plasma treated silicon substrate has an RMS roughness of 2–3 nm (29).

RESULTS

The measured force between silica surfaces immersed in solutions of 5.0×10^{-6} M CPCI in 0.1 M NaCl, normalized by the radius of the probe, is shown in Fig. 2. This concentration of CPCI is about 1/20 of the critical micelle concentration (CMC) of $\sim 1.0 \times 10^{-4}$ M in 0.1 M NaCl. As the surfaces approach no interaction is seen until they are within 25 nm, where a sudden jump into contact occurs as the gradient of the attractive force exceeds the spring constant of the cantilever. This jump is indicated by an arrow the

slope of which is the spring constant divided by the probe radius. The high background salt concentration screens any electrostatic DLVO component of the force. The range and magnitude of this attraction exceeds the van der Waals (vdW) interaction expected between these surfaces. This is consistent with the presence of a fairly complete monolayer adsorbed at each silica surface, leading to a hydrophobic attraction between the surfaces.

The jump distances varied considerably and fall naturally into two categories, defined by the force profile seen upon separation. Curves of both categories were seen within an experiment in the same interaction region. The approaches exhibiting smaller jumps of between 20 and 45 nm behaved as shown in Fig. 2 and demonstrated a “normal” adhesion. Approaches exhibiting larger jumps of greater than 55 nm (jumps of between 45 and 55 nm were not seen) differed considerably on separation, as seen in Fig. 3. In this case, no interaction is seen until the surfaces approach to within 85 nm, where a sudden jump into contact occurs. Upon separation, a strongly attractive force is seen going through a maximum at approximately 300 nm and extending to greater than 1450 nm, where it becomes repulsive. The surface separation is controlled by a piezo crystal the range of which could not extend further. When the separation between the surfaces was reduced the force followed the curve seen upon retraction. If however, the surfaces are separated

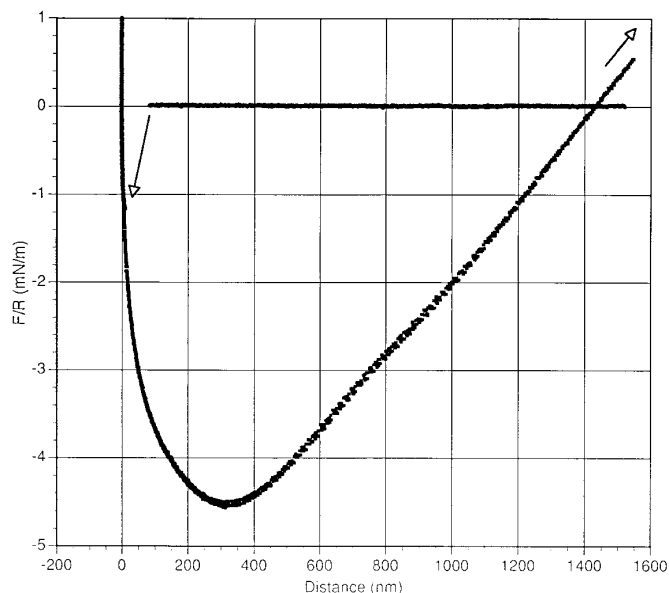


FIG. 3. An interaction curve measured on approach and separation between silica surfaces immersed in a solution of 5.0×10^{-6} M CPCI and 0.1 M NaCl for the same region of interaction as seen in Fig. 2. On approach no interaction is seen until a sudden jump into contact occurs from approximately 70 nm (see arrow). This jump distance is much larger than that shown in Fig. 2. On separation a bridging cavity is formed between the surfaces, leading to a strong adhesion and at greater than 1450 nm a repulsion. The surfaces are still interacting beyond this separation, which is limited by the range of the piezo tube.

to approximately $50 \mu\text{m}$ or greater, and then the run repeated no interaction was seen until a sudden jump occurred as observed on the original approach. These observations are consistent with the formation of a bridging bubble or cavity between the surfaces. Once a cavity had formed between the surfaces and “survived” separation to a given distance the cavity was found to be stable and remained even after several hours. Interactions as shown in Fig. 2 occurred both before and after interactions of the type shown in Fig. 3. This variation is discussed later.

At a concentration of $0.001 M$ CPCl, which is slightly above the CMC of $0.9 \times 10^{-3} M$, an electrostatic repulsion is observed as shown in Fig. 4. This is due to the formation of a charged bilayer on each silica surface. After the bilayers are brought into contact a steep repulsion is evident. Upon further increase in the applied force, the surfaces approach a further 6 nm , approximately the thickness of two bilayers. After this point the scatter in the data increases dramatically as a bubble or cavity is formed. This extreme increase in noise is likely due to vibration of the tip arising from contact of the probe with a vapor/liquid interface. The distance information in this region is not reliable. The data points are shown merely to illustrate the formation of a bubble or cavity, in this case while the surfaces are being pushed together. Upon retraction, the noise level remains high and a large attraction is evident (not shown in figure). The interaction on approach can be fitted to a double layer force with a

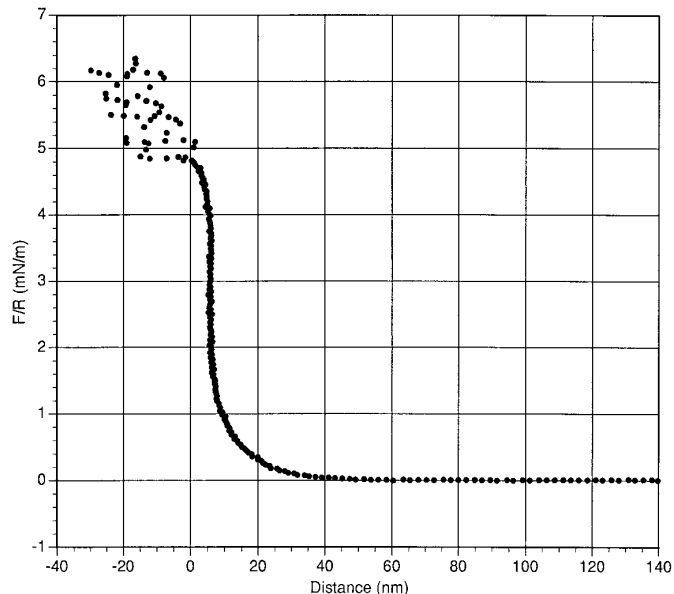


FIG. 4. Interaction curve measured on approach between silica surfaces in a solution of $0.001 M$ CPCl. At this concentration, which is slightly above the CMC, a bilayer forms on each silica surface. The charge on the bilayer gives rise to a DLVO repulsion prior to contact. Subsequently, bilayer rupture is seen as the surfaces approach by a further 6 nm , prior to a steep repulsion. As the surfaces are further forced together the scatter in the data is seen to increase suddenly. The data in this region are unreliable but illustrate the presence of a cavity or bubble between the surfaces.

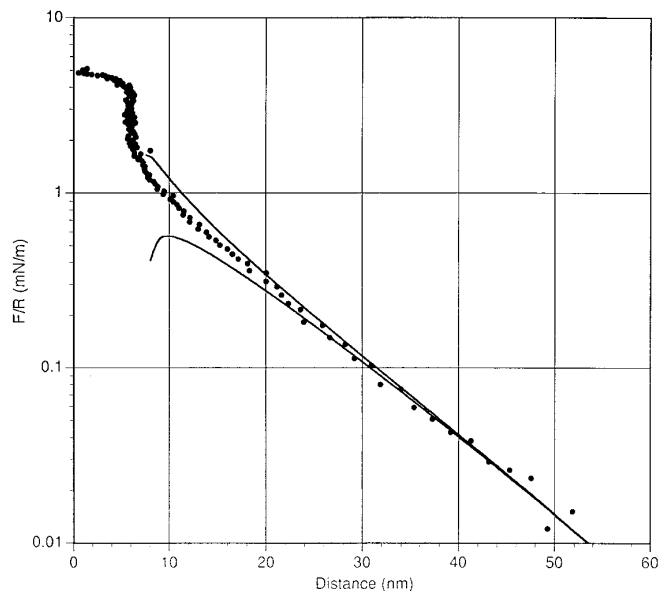


FIG. 5. Interaction curve measured on approach between silica surfaces in a solution of $0.001 M$ CPCl. The upper and lower solid lines were calculated using a numerical solution to the Poisson–Boltzmann equation (30) for boundary conditions of constant surface charge (upper) and constant surface potential (lower). The vdW force was included as a nonretarded interaction with a Hamaker constant of $8.5 \times 10^{-21} \text{ J}$. The fit is achieved using a potential of 42 mV and an expected Debye length of 9.6 nm , displaced to the plane of the bilayer (6 nm). At high force the rupture of the bilayer is seen as the surfaces approach by a further 6 nm .

potential of $+42 \text{ mV}$ and an expected Debye length of 9.6 nm ; see Fig. 5. Here the steep repulsion arising from bilayer/bilayer contact has been used as the zero distance for both vdW and electrostatic components of the theoretical fit. At greater applied force, the rupture of the bilayers is seen and the surfaces are able to approach by a further 6 nm . The upper and lower solid lines were calculated using a numerical solution to the Poisson–Boltzmann equation (30) for boundary conditions of constant surface charge (upper) and constant surface potential (lower). The vdW force was included as a nonretarded interaction with a Hamaker constant of $8.5 \times 10^{-21} \text{ J}$. The $+42 \text{ mV}$ potential corresponds to an area per charge of 47 nm^2 . For a head group area of 0.4 nm^2 the effective dissociation of chloride ions is found to be low at only 0.9% .

Similarly to the monolayer system, the formation of a cavity was not seen between bilayers on every occasion. However, unlike the monolayer system, the formation of a cavity between the surfaces could be controlled. Cavity formation was avoided by limiting the force with which the bilayers were pushed together. At higher forces the bilayers would rupture, leading to the formation of a cavity upon separation. A series of force runs were conducted with increasing applied force (F/R) from 1 to 5.5 mN/m . At 5.5 mN/m the applied force proved sufficient to rupture the bilayers and form a cavity. Figure 6 shows the penultimate

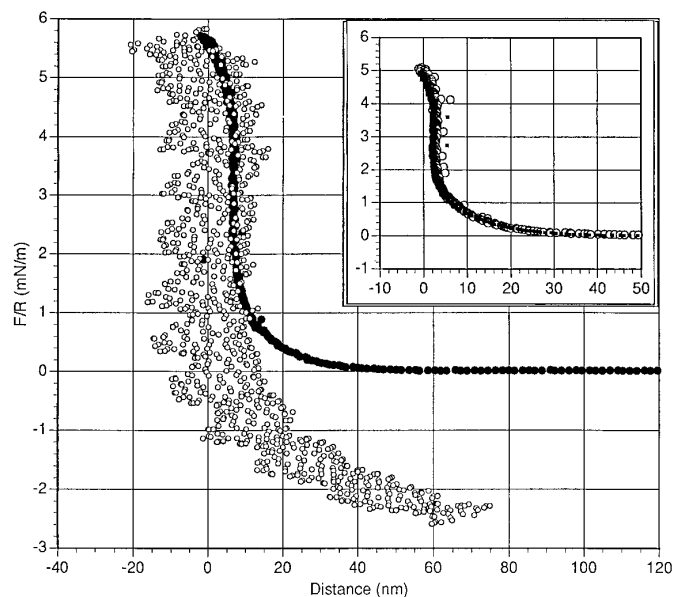


FIG. 6. Interaction curve measured between silica surfaces in a solution of 0.001 *M* CPCl. The charge on the bilayer gives rise to a DLVO repulsion. As the bilayers are forced together a steep repulsion is seen prior to the deformation and complete rupture of the bilayers. The surfaces approach by a further 7 nm as the bilayers on both surfaces are squeezed out. Upon separation the noise in the data is dramatically increased. The data in this region are unreliable but illustrates the presence of a cavity or bubble between the surfaces. The inset shows the interaction on approach and separation for the immediately previous run. The applied force is slightly less and insufficient to completely disrupt the bilayers. A softness at high driving force leads to a compression of about 3 nm. This corresponds to the semirupture of each bilayer as a monolayer is removed from each surface, leaving a single bilayer separating the surfaces. No cavity formation is seen.

(inset) and ultimate runs in this series. The final run exhibits an electrostatic repulsion followed by a steep repulsion arising from bilayer/bilayer contact before a region where the bilayers are compressed by approximately 7 nm, leading to their total disruption and the formation of a cavity upon separation, as evidenced by the noise in the data. Again these data are unreliable but serves to indicate the presence of a cavity. The previous approach (shown in Fig. 6 inset) exhibits similar characteristics but the force applied is less and the bilayers are only compressed by about 3 nm. This compression can be interpreted as disruption of the two bilayers to form a single bilayer (or a monolayer at each surface). This behavior for adsorbed surfactants has previously been reported by workers using the Surface Forces Apparatus (SFA) (13, 31). Upon separation, the disruption to the surface layers is quickly reversed and the same force versus distance profile as on approach is followed.

Figure 7 shows a force vs distance profile upon separation where a bridging cavity has formed and the noise level has remained sufficiently low to allow the data to be analyzed. The force at small separations is strongly attractive. A contact angle of $\theta > 90^\circ$ is required to give an attractive capillary

force. At separations greater than approximately 1200 nm the measured force becomes repulsive. This can occur if the contact angle becomes less than 90° or as is more likely, the curvature becomes dominated by the radius of curvature in the plane parallel to the flat surface (where the surface is curved towards the cavity), leading to a change in the sign of the Laplace pressure. The inset in Fig. 7 again shows the force measured on separation when a bridging cavity is present; however, at a separation of approximately 900 nm, the bridging cavity breaks and the measured force returns to zero.

Advancing and receding contact angles were measured by the sessile drop method. A solution of 5×10^{-6} *M* CPCl and 0.1 *M* NaCl initially wetted the freshly plasma treated silicon surface and then receded over about 20 s as a monolayer of surfactant was deposited. The advancing contact angle was initially below 50° but increased over 2 h to give an advancing angle of $60.5 \pm 1^\circ$ and a receding angle of $31.5 \pm 1.5^\circ$ on a plasma treated silicon surface. The same solution on a glass slide, cleaned by soaking in 10 wt% NaOH, gave a much lower advancing contact angle, around 23° . However, in a solution containing a slightly increased CPCl concentration of $\sim 5.5 \times 10^{-6}$ *M* and 0.1 *M* NaCl, the contact angle was found to have immediately increased to $\sim 43^\circ$. This indicates that the solution was just above the minimum concentration that would form a monolayer on the silica surface used in the force experiments. A solution of 0.001 *M* CPCl gave an advancing angle of $51 \pm 1^\circ$ and a receding angle of $< 5^\circ$ on a plasma treated silicon surface.

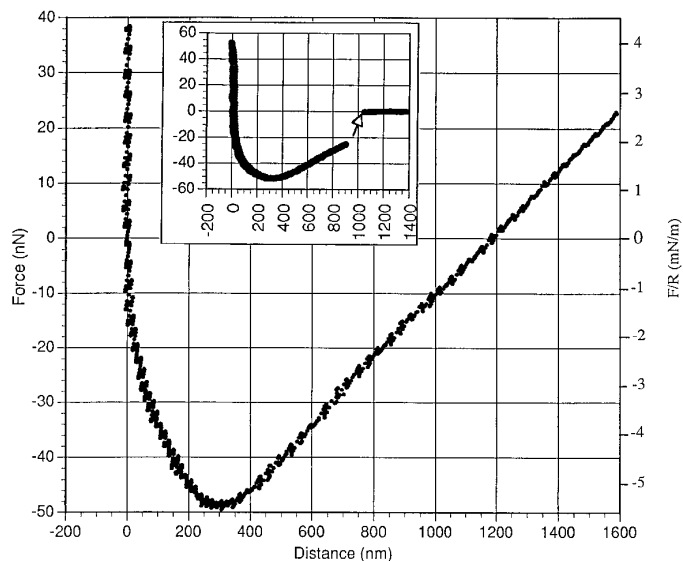


FIG. 7. Interaction curve measured upon separation between silica surfaces in a solution of 0.001 *M* CPCl. A bridging cavity has formed giving rise to a strong attraction which eventually becomes repulsive. The experimental forces measured here have been used to derive the principal radii in Fig. 9. The inset shows the measured force profile upon separation when a cavity is initially present but ruptures upon separation.

DISCUSSION

Monolayer Coated Silica Surfaces

Measurements of the long range, non-DLVO attraction between hydrophobic surfaces were first reported by Pashley and Israelachvili (13) in 1981, and have since been repeated by many workers using a wide variety of substrates. The molecular origins of the interaction are as yet unclear and much debated (32–35). The variation in jump distances seen in this work is not new (36), and may be due to true random variation in the magnitude and range of the force rather than any local variation in surface hydrophobicity. That cavities were only observed for force curves exhibiting the larger jump distances suggests that the formation of the cavity is related to the attraction between the surfaces. This could arise simply because larger jumps may lead to a greater impact between the surfaces, favoring cavity formation. However, the formation of a bridging bubble has been posed as a possible mechanism for the hydrophobic attraction (35, 37, 38). Perhaps then a bubble is formed between the surfaces on approach and is only revealed upon separation. It is possible that the formation of a cavity may be the cause of all the attractive jumps, but only the cavities associated with the larger jumps remain to be seen upon retraction. Very small cavities may not be revealed by the optical fringes of the surface forces apparatus (SFA).

The range of the attractive force seen in this work, up to 85 nm, is surprisingly large given the nature of the surface and the contact angle. Generally, forces measured between surfaces that have been formed by equilibrium adsorption of surfactant, as used here, are of short range (<10 nm). However, recently a similarly long-ranged attraction has been measured using CTAB adsorbed to silica surfaces in low salt solutions (39). In addition, the surfaces used here are only moderately hydrophobic (advancing angle 60°) in comparison to other surfaces used. An advancing contact angle of 60° is lower than expected for a pure hydrocarbon surface. This is most likely due to the presence of impurities. Small amounts of impurities have had similar effects on CTAB coated mica surfaces (14). Before an adequate explanation can be made as to why the attraction here is long ranged, a better understanding of the nature of the attraction is required. The high salt level used in these experiments would appear to preclude an electrostatic mechanism.

Bilayer Coated Silica Surfaces

The surface potential obtained by fitting theoretical DLVO curves to the measured forces in 0.001 M CPCl yields a potential for the bilayer of +42 mV as shown in Fig. 5. This potential is low in comparison to the potential of +80 to +90 mV obtained for CTAB (40) (cetyltrimethylammonium bromide) and +110 mV obtained for CTAC (41) (cetyltrimethylammonium chloride) on silica. The lower potential

measured here can be attributed to the different chemical nature of the head group. Also, the surface roughness and impurities (42) are likely to affect the potential. The adsorption of cationic surfactants onto silica surfaces yields lower surface potentials than those obtained for mica surfaces. There are several possible causes of this phenomenon. CTAB adsorbs to mica by an ion exchange mechanism that theoretically can occur in a 1:1 ratio, giving a tightly bound cationic surfactant monolayer and subsequently a tightly packed, high potential bilayer. In contrast to the crystalline mica, silica surfaces carry two distinct types of surface hydroxyl sites, single sites and geminal sites (43), presumably in a disordered array. Due to the size of the surfactant head group it is impossible for every silica site to be occupied and given the amorphous nature of silica it is reasonable to expect that a tightly packed monolayer is difficult to form. This in turn would lead to a loosely packed bilayer. Furthermore, the dissociation of the geminal sites is likely to be affected by the immediate chemical environment. The plane of the silica surface may retain a net negative charge as seen in zeta potential measurements of methylated silica surfaces (44). If this were true then it would directly lower the magnitude of the repulsion measured between the surfaces and resemble a system with a lower potential at the surface of the bilayer. The surface roughness of silica as compared to the molecularly smooth cleaved mica surfaces may also affect the ability of cationic surfactants to form a tightly packed layer. The discrepancy in the measured potentials using silica and mica substrates is discussed at length by Rutland and Parker (40), who conclude that CTAB forms surface aggregates, either patches of bilayers or flattened micelles, on silica surfaces as opposed to true bilayers on mica surfaces. This contention is supported by the recent work of Manne and Gaub (45). The lower potentials seen in this work would suggest that the CPCl aggregates at the surface are even less tightly packed than those composed of CTAB. This may arise as a result of restricted rotation about the N–C₁ bond in CPCl (46) leading to packing constraints.

Previous workers have looked at the rupture of surface aggregates using the surface forces apparatus (SFA) in solutions of CTAB (13, 40) and phosphatidylcholine (31). All were able to disrupt the bilayers by squeezing out a monolayer from each surface, but were unable to exclude both bilayers even at F/R values far greater than those sufficient to completely rupture the bilayer in this work. When mica was used as a substrate, even at forces sufficient to locally flatten the mica substrate the bilayer was not completely ruptured. The small radius of the probe used here (11.3 μm) may allow rupture to occur more easily but the loose packing of the bilayer is likely to be the main factor leading to complete bilayer rupture. Additionally, surface roughness and impurities (31) are likely to favour bilayer rupture. Further, the fluidity of the bilayer may be important. CTAB has a Krafft temperature close to room temperature, which is

considerably higher than CPCl. Adsorption to a substrate may induce crystallinity upon the hydrocarbon tails of CTAB. Any estimate of force or pressure required to rupture a cell membrane must take into account the presence of membrane proteins, cell coatings such as the glycocalyx, cell stiffness, curvature and the precise chemical composition of the membrane. Therefore, no such estimate can be made from this work.

Cavity Formation by Tribonucleation

The capillary force generated between the probe and the flat upon bilayer rupture is shown in Fig. 7 as a function of separation. Marmur has calculated by numerical solution and by an approximate analytical equation the capillary force, given (i) the radius of the probe, (ii) the contact angle, and (iii) the surface separation (47). This is derived for the case of a drop of liquid between two solid surfaces in air, but is equally applicable to a gas phase between two solid surfaces in a liquid. If the principal radii of curvature (R_1 and R_2) of the capillary and the surface tension of the solution, σ , are known the pressure difference across the interface can be calculated using the Young–Laplace equation,

$$\Delta P = \sigma(1/R_1 - 1/R_2). \quad [1]$$

The attractive force, F , due to the capillary can then be calculated by

$$F = -\pi x^2 \Delta P, \quad [2]$$

where x is the radius of the circle defined by the perimeter of the capillary, in contact with the surface. Using a numerical solution, Marmur has been able to test the validity of the analytical approximation for different contact angles. For

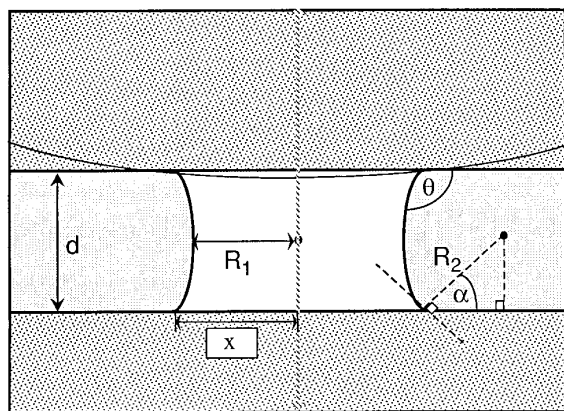


FIG. 8. Schematic diagram of a bridging cavity between two flat surfaces. R_1 and R_2 are the principal radii of curvature in the planes parallel and perpendicular to the surfaces respectively. θ is the contact angle, d is the separation, and $\alpha = (\theta - 90^\circ)$. x is the radii of the circle of contact described by the meniscus. The meniscus is assumed to be axisymmetric.

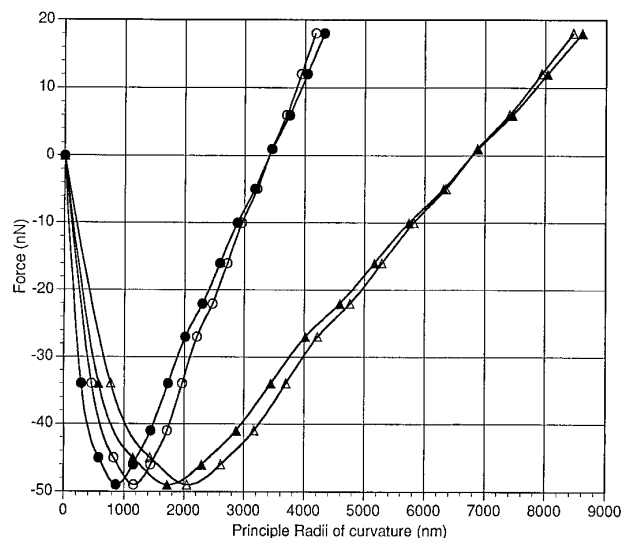


FIG. 9. Calculated principal radii of curvature (plotted against force) in the planes parallel (R_1 ; filled) and perpendicular (R_2 ; unfilled) to the surfaces, using Eq. [3] and the force data from Fig. 7 for contact angles of 95° (triangles) and 100° (circles). The surface tension used in the calculations is 40 mJ/m^2 , the capillary is assumed to be symmetric, and hydrostatic effects have been ignored.

low contact angles the approximation is good but as the contact angle approaches 90° the approximation is very poor. An alternative, simplified approach is to look at the case of a capillary between two flat surfaces as shown in Fig. 8. Using the experimentally measured force (F) and setting $x \approx R_1$, an approximate value for R_1 can be found by solving the equation

$$0 = R_1^2 - R_2 R_1 - FR_2/(\pi\sigma). \quad [3]$$

By simple geometry $R_2 = d/2 \sin \alpha$, where d is the separation of the surfaces and $\alpha = (\theta - 90^\circ)$, where θ is the contact angle. The results of this calculation, using the experimental force data from Fig. 7, are shown in Fig. 9 for contact angles of 95° and 100° .

This approach, though crude, reveals several interesting features. From the principal radii an approximate volume of the cavity can be calculated. It is found that the volume increases sharply with separation even in the regime where the force becomes repulsive. On occasion the capillary is seen to break as the force on separation is seen to suddenly return to zero as shown in the inset of Fig. 7. From Fig. 9 it can be seen that on separation R_1 continues to grow and will eventually approach the radius of the spherical probe. This is unphysical for the flat/sphere geometry and rupture of the cavity may occur when R_1 grows too large. This mechanism is supported by the observation that cavities once formed were stable, provided the separation between the surfaces was not increased. When the capillary does break there is no evidence that a bubble remains on either of the

surfaces. If a bubble adhered to the probe, a hydrodynamic force would be detected and if a bubble remained on the flat substrate the following approach would reveal a change in the force profile. It must be then assumed that the cavity disintegrates. This suggests that the cavity contains largely water vapor rather than a gas that has diffused from solution. Although the calculation is performed using a single value for the contact angle it is unlikely that the contact angle is in reality static, given the expansion of the cavity. For the different geometry of a sphere and a flat, a cavity behaving similarly to the simple model will have a dynamic contact angle, at least with the spherical probe.

It would appear that for a capillary force to give rise to the experimental force profiles measured here, a contact angle in excess of 90° is required. However, the contact angles measured are well below this. The difference is difficult to reconcile. It is possible that the surfaces are inhomogeneous, perhaps due to the presence of impurities, and that in local regions the contact angle is much higher than the macroscopically measured values. This is supported by the variable jump distance seen between monolayer surfaces and the correlation between jump distance and cavitation, though this could be due to the nature of the hydrophobic interaction. As discussed earlier, the packing of surfactant at the surfaces is unlikely to be the maximum allowable by physical packing constraints. The forcing together of the surfaces may momentarily cause a greater packing density, which may give rise to a higher contact angle. This is perhaps more likely between ruptured bilayers than for the hydrophobic surfaces covered by a monolayer.

The cavities formed between the ruptured bilayer surfaces or between the monolayer surfaces were found to be stable even after many hours, provided the surface separation was not greatly increased. This would suggest that once such cavities form in the body they would exist for days and perhaps weeks. Cavities formed by tribonucleation within the body are likely to be further stabilized by the "organic skin effect," whereby organic molecules in solution adsorb at the liquid/gas interface (48) and in doing so stabilize it against dissolution by limiting gas transfer across the interface (49). Once a cavity has acquired a protein shell its dissolution is greatly slowed. Furthermore, if the cavity subsequently disappears the protein shell itself may be capable of nucleating bubbles (50).

If cavities formed by tribonucleation are the nucleation sites responsible for bubble formation leading to decompression sickness, then a significant population of cavities must be present in the body. It is difficult to estimate the rate of production of cavities in the body, but if a few are created with every considerable muscular movement and the nuclei have an extended lifetime, then a population capable of giving rise to a large number of bubbles may exist. It is likely that many bubbles can be produced from any one nucleus. An example of this is the stream of bubbles produced in a

glass of beer or champagne. Nuclear fission of ^{238}U present in the body has been proposed as the source of nuclei responsible for decompression sickness (10), where the calculated rate of fission leads to one disintegration occurring every three weeks. It appears unlikely that nuclear fission from bodily uranium could give rise to sufficient nuclei to produce the numerous bubbles formed during decompression sickness, but the formation of micronuclei during everyday activities, by tribonucleation, may lead to the presence of many bubble nucleating sites in the body.

SUMMARY

A long range hydrophobic attraction, varying in magnitude and range, is seen between monolayers of CPCI adsorbed onto silica from aqueous solution. The surfaces were seen to jump into contact from separations between 20 and 85 nm. Upon separation, a bridging cavity is seen to form when the attractive jump into contact exceeds 55 nm. Above the CMC, bilayers of CPCI form on each silica surface and the interaction forces are well described by DLVO theory. The fitted potential using the nonlinear Poisson-Boltzmann equation is consistent with a loosely packed bilayer. The force on separation is dependent upon the damage incurred by the bilayers when they are forced together. At high forces the bilayers are completely ruptured and a bridging cavity is formed. An analogy is drawn between these bilayers and cell membranes and it is postulated that rupture of cell membranes could lead to the formation of cavities *in vivo*. Such cavities are likely to provide the nucleation sites responsible for the formation of bubbles causing decompression sickness.

ACKNOWLEDGMENTS

I thank Carinna Tong for fruitful discussions and much appreciated assistance, and Professors Ric Pashley and Barry Ninham for supervision and support. Thanks also to Dr. Tim Senden for many helpful suggestions during the preparation of this manuscript and Anthony Hyde for technical assistance and the artwork in Fig. 1. This work has been supported by an Australian Research Council grant.

REFERENCES

- Gillis, M. F., Karagianes, M. T., and Peterson, P. O., *J. Occup. Med.* **11**, 245 (1969).
- Fisher, J. C., *J. Appl. Phys.* **19**, 1062 (1948).
- Gerth, W. A., and Hemmingsen, E. A., *J. Colloid Interface Sci.* **74**, 80 (1980).
- Hemmingsen, E. A., *Science* **167**, 1493 (1970).
- Hemmingsen, E. A., *J. Appl. Phys.* **46**, 213 (1975).
- Evans, A., and Walder, D. N., *Nature* **222**, 251 (1969).
- Harvey, E. N., Barnes, D. K., McElroy, W. D., Whiteley, A. H., Pease, D. C., and Cooper, K. W., *J. Cell. Comp. Physiol.* **24**, 1 (1944).
- Harvey, E. N., Whiteley, A. H., McElroy, W. D., Pease, D. C., and Barnes, D. K., *J. Cell. Comp. Physiol.* **24**, 23 (1944).
- Harvey, E. N., *J. Am. Chem. Soc.* **67**, 156 (1945).
- Walder, D. N., and Evans, A., *Nature* **255**, 696 (1974).

11. Ikels, K. G., *J. Appl. Physiol.* **28**, 524 (1970).
12. Wentzell, R. A., *Phys. Rev. Lett.* **56**, 732 (1986).
13. Pashley, R. M., and Israelachvili, J. N., *Colloids Surf.* **2**, 169 (1981).
14. Israelachvili, J. N., and Pashley, R. M., *Nature* **300**, 341 (1982).
15. Rabinovich, Y. A. I., and Derjaguin, B. V., *Colloids Surf.* **30**, 243 (1988).
16. Pashley, R. M., McGuiggan, P. M., Ninham, B. W., and Evans, D. F., *Science* **229**, 1088 (1985).
17. Christenson, H. K., and Claesson, P. M., *Science* **239**, 390 (1988).
18. Shaker, L. A., Russell, A. D., and Furr, J. R., *Int. J. Pharm.* **34**, 51 (1986).
19. Quisno, R. A., and Foter, M. J., *J. Bacteriology* **52**, 111 (1946).
20. Shelton, R. S., Van Campen, M. G., Tilford, C. H., Lang, H. C., Nisonger, L., Bandelin, F. J., and Rubenkoenig, H. L., *J. Am. Chem. Soc.* **68**, 757 (1946).
21. Hall, M. J., and Sukan, S. S., *Haceteppe Bull. Nat. Sci.* **1**, 10 (1972).
22. Jurkiewicz, K., and Waksmundzki, A., *Rocz. Chem.* **47**, 1457 (1973).
23. Walkowiak, W., and Bartecki, A., *Nukleonika* **18**, 133 (1973).
24. Meyer, G., and Amer, N. M., *Appl. Phys. Lett.* **53**, 1045 (1988).
25. Alexander, S., Hellemans, L., Marti, O., Schneir, J., Elings, V., Hansma, P. K., Longmire, M., and Gurley, J., *J. Appl. Phys.* **65**, 164 (1989).
26. Ducker, W. A., Senden, T. J., and Pashley, R. M., *Langmuir* **8**, 1831 (1992).
27. Ducker, W. A., Senden, T. J., and Pashley, R. M., *Nature* **353**, 239 (1991).
28. Cleveland, J. P., Manne, S., Bocek, D., and Hansma, P. K., *Am. Inst. Phys.* **64**, 1 (1993).
29. Senden, T. J., and Ducker, W. A., *Langmuir* **8**, 733 (1992).
30. Chan, D. Y. C., Pashley, R. M., and White, L. R. J., *J. Colloid Interface Sci.* **77**, 283 (1980).
31. Horn, R. G., *Biochim. Biophys. Acta* **778**, 224 (1984).
32. Podgornik, R., *J. Chem. Phys.* **91**, 5840 (1989).
33. Eriksson, J. C., Ljunggren, S., and Claesson, P. M., *J. Chem. Soc. Faraday Trans. II* **85**, 163 (1989).
34. Ruckenstein, E., and Churaev, N., *J. Colloid Interface Sci.* **147**, 535 (1991).
35. Bérard, D. R., Attard, P., and Patey, G. N., *J. Chem. Phys.* **98**, 7236 (1993).
36. Meagher, L., and Craig, V. S. J., *Langmuir* **10**, 2736 (1994).
37. Parker, J. L., Claesson, P. M., and Attard, P., *J. Phys. Chem.* (1994).
38. Christenson, H. K., and Claesson, P. M., *Science* **239**, 390 (1988).
39. Kékicheff, P., and Spalla, O., *Phys. Rev. Lett.* **75**, 1851 (1995).
40. Rutland, M. W., and Parker, J. L., *Langmuir* **10**, 1110 (1994).
41. Johnson, S. B., Drummond, C. J., Scales, P. J., and Nishimura, S., *Colloids. Surfs.* **103**, 195 (1995).
42. Pashley, R. M., and Israelachvili, J. N., *J. Colloid Interface Sci.* **98**, 500 (1984).
43. Hair, M. L., and Hertl, W., *J. Phys. Chem.* **73**, 2372 (1969).
44. Laskowski, J., and Kitchener, J. A., *J. Colloid Interface Sci.* **29**, 670 (1969).
45. Manne, S., and Gaub, H. E., *Science* **270**, 1480 (1995).
46. Weiss-Lopez, B. E., Gamboa, C., and Tracey, A. S., *Langmuir* **11**, 4844 (1995).
47. Marmur, A., *Langmuir* **9**, 1922 (1993).
48. Bachhuber, C., and Sanford, C., *J. Appl. Phys.* **45**, 2567 (1974).
49. Manley, D. M. J. P., *Br. J. Appl. Phys.* **11**, 38 (1960).
50. Berge, L. I., *J. Colloid Interface Sci.* **134**, 548 (1990).